A Simple Unconventional Plasticity Model Within the Multilaminate Framework

S. A. Sadrnejad[1,*], S. A. Ghoreishian Amiri[2]

Received: August 2008 Accepted: November 2009

Abstract: *A semi-micromechanical multilaminate model is introduced here to predict the mechanical behavior of soils. This model is like a bridge between micro and macro scale upon the satisfaction of minimum potential energy level during any applied stress/strain increments. The concept of this model is based on a certain number of sampling planes which constitute the elastic-plastic behavior of the soil. The soil behavior presents as the summation of behavior on these planes. A simple unconventional constitutive equations are used in each of the planes to describe the behavior of these planes separately. An unconventional plasticity can predict the soil behavior as a smooth curve with considering plastic deformation due to change of stress state inside the yield surface. The model is capable of predicting softening behavior of the soil in a reasonable manner due to using unconventional plasticity. The influences of induced anisotropy are included in a rational way without any additional hypotheses owing to in-nature properties of the multilaminate framework. Results of this model are compared with test data and reasonable agreement is found.*

Keywords: *multilaminate models, unconventional plasticity, anisotropy, softening behavior*

1. Introduction

Geomaterials consisting of grains in contact and surrounding voids are particulate media that mostly are considered as continuum media for ease. So the accurate behavior of such particulate materials has to be investigated through micromechanics. However, the micro-mechanical behavior of geomaterials is inherently discontinuous and heterogeneous.

The macroscopic as an overall or averaged behavior of granular materials is determined not only how discrete grains are arranged through medium, but also by what kinds of interactions are operating among them. To investigate the micro-mechanical behavior of geomaterials, certainly, the spatial distribution of contact points and orientation of grains must be identified. In engineering point of view, the main goal is formulating macro-behavior of granular materials in terms of micro-quantities. However, there exist two well-known theories that explain the relation between micro-fields and macro-fields as macro-micro relations, in a consistent manner as the average field theory and the homogenization theory.

For a geomaterials such as sand that supports the overall applied loads through contact friction, the overall mechanical response ideally may be described on the basis of micro-mechanical behavior of grains interconnections. Naturally, this requires the description of overall stress, representation of kinematics, development of local rate constitutive relations and evaluation of overall differential constitutive relations in terms of the local quantities. Representation the overall stress tensor in terms of micro level stresses and the condition, number and magnitude of contact forces has long been the aim of numerous researchers [1, 2].

Multilaminate models by defining the small continuum structural units as an assemblage of solids and voids that fill infinite spaces between the sampling planes, has appropriately justified the contribution of interconnection forces in overall macro-mechanics. Upon these assumptions, plastic deformations are to occur due to sliding, separation/closing of the boundaries of the small continuum units and elastic deformations are the overall responses of structural unit bodies.

When load is applied on the soil mass, contact forces between adjacent particles develop which

* *Corresponding Author: Email: sadrnejad@kntu.ac.ir*

1 *Professor, Civil Engineering Department, K.N.Toosi University of Technology, Tehran, Iran*

2 *PhD student, Civil Engineering Department, K.N.Toosi University of Technology, Tehran, Iran Email: sa_ghoreishian@dena.kntu.ac.ir*

can be divided into normal and tangential components. In the initial stress state these contacts and bounds depend on the history the soil has undergone prior to construction activities. The overall deformation behavior of soils results from both deformation of individual particles and relative sliding between particles. The inter-particle sliding which is governed by the shear resistance at contacts between the particles makes the major contribution to the overall strain and this contribution is accounted for in the multilaminate models. Since the individual particles are not modeled in a discrete way, the interactions between particles are considered in an average form on contact planes. Rotation of individual grains cannot be explicitly modeled. Number, direction and orientation of the planes are governed by numerical integration rules. It is assumed that the individual planes do not interact and usually the same mathematical relations hold for all planes. However, this assumption is not strictly required and initial anisotropy may be easily introduced by varying parameters over the plane prior to loading.

Depending on the stress path while loading, certain integration planes will behave individually, and therefore, induced anisotropy which depends on the stress path is automatically accounted for. Rotations of principal stress axes which generally take place in boundary value problems can be simulated in a simple and physically meaningful way. The capabilities of the multilaminate framework to respond to stress path which the principal stress axes rotate have been demonstrated previously by Schweiger and Schuller [3].

The first multilaminate model for joint rocks has been proposed by Zeinkiewicz and Pande [4]. They have supposed that a pronounced anisotropy of rock can be represented by introducing a limited number of planes of weakness, typically two or three. On these planes the constitutive model can be formulated in local coordinates describing the amount of sliding and opening which in turn governs the overall behavior of jointed rock. This approach has been implemented into finite element codes also by others and is successfully used in solving problems in practical rock engineering.

Pande and Sharma [5] introduced the multilaminate concept for clays and formulated a critical state model on contact planes. A multilaminate model for sand including shear and volumetric hardening has been presented by Krajewski [6]. A different formulation for sands has been suggested by Sadrnejad and Pande [7]. Above formulation have been implemented into finite element codes employing a (pseudo)-viscoplastic algorithm, i.e. viscoplasticity and have been used for solving the non-linear equation system but no true time dependent behavior has been included. Another plasticity formulation of the multilaminate model has been introduced by Pietruszczak and Pande [8]. More recent developments of the multilaminate model include research on strain localization in dense sands has been proposed by Karstunen [9] where a plasticity formulation of the multilaminate model with deviatoric hardening and a non-associated flow rule has been used. A similar approach has been developed in modeling fracture propagation in concrete as well as the behavior of geomaterials, is the microplane model; presented by Bazant and Prat for the first time [10].

Another point in the multilaminate based model is the constitutive equations which used in each plane for describing sliding, separation/closing of the boundaries. The common formulations to describe sliding, separation/closing of these planes have been introduced in the conventional plasticity framework. Conventional plasticity is based on the idealization that the interior of the yield surface is a purely elastic domain. Conventional elastoplasticity has contributed greatly to prediction of hardening behavior in metals and normally consolidated soils. This idealization would not lead to unrealistic prediction of the hardening behavior of materials. However, it would cause unrealistic prediction of softening behavior, in that the stress state tends to decrease abruptly when reaches the yield surface. Therefore, unconventional elastoplasticity would have to adopt for predicting softening behavior: this does not use the idealization of conventional elastoplasticity, and thus make it possible to describe the plastic deformation due to the

change of stress inside the yield surface. In other word there is no purely elastic domain inside of the yield surface. So it can exhibit a smooth elastic-plastic transition.

Various models which are falling within the framework of unconventional elastoplasticity have been introduced: the multi-surface model [11, 12, 13], the infinite surface model [14], the two surface model [15, 16] and the subloading surface model [17, 18, 19]. Among of these, the subloading surface model has the simplest form. It adopts the associated flow rule and fulfils the fundamental mechanical requirements: the continuity condition, the smoothness condition and the work rate-stiffness relaxation, as reviewed in detail by Hashiguchi [20, 21, 22, 23].

In this study, a simple subloading surface model has been developed within the multilaminate framework for more realistic prediction of soil deformation. Developing the subloading surface model in the multilaminate framework, the purposed model can describe the influence of anisotropy and rotation of principal stress axis in a rational way without any additional hypotheses. However, scholars attempted to consider these phenomena in the subloading surface model with defining rotational hardening [24]. This supposition changes the simple subloading surface model to a complicated one.

Throughout this paper the stress and strain are taken positive for compression, and the stress for soils is taken as *effective stress.*

2. Strain Distribution Around a Point

In continuum mechanics, it is convenient to define the strain distribution at a point, with considering its components on the outer surface of a typical *dx, dy, dz* element. Consequently the solution will consider uniform and homogeneous strain components distribution over the outer surface of such *dx, dy, dz* element on three perpendicular coordinate axes.

Because of slippage, widening and closing between granular medium particles, there is a requirement of a further consideration for modeling of the displacements of these mediums in a more rational way. This will cause a new contribution to strain in addition to that is caused from the compression of particles.

Now consider two neighboring points on both side of the contact point of two particles. In general these two points do not remain close to each other but they can describe complex trajectories. Fictitious average points belong to the fictitious continuous media can be defined remaining adjacent so as to define a strain tensor. The problem will be different for disordered particles compared with ordered equal size spheres. There might be small zones with no relative movement of particles, in this case. This could lead to specific behavior such as periodic instabilities known as slip-stick which creates non-homogeneity in strains and displacements of the medium.

In the solving of a non-linear problem, the mechanical behavior depends strongly on stress/strain path and their histories. Upon these conditions, considering the strain components along three perpendicular coordinate axes may not reflect the real historical changes during the loading procedure. In the most extreme cases, one can define a sphere shape element with radius *dr* (instead of cube with *dx, dy, dz*) which carrying the distributed strain on its surface, can reflect strain components on infinite orientations at a point when dr tends to zero.

The finite strain at any point in three dimensions by coordinates (*x, y, z*) is defined with the displacements of the sides of an initial rectangular-coordinate box with sides of length dx, dy and dz to form the sides of a parallelepiped as shown in Fig. 1a. One can establish this configuration of strain by considering the displacements of the corner points (x, 0, 0), (0, y, 0) and (0, 0, z). This kind of strain approach leads to define a (3×3) strain tensor including six components to present the displacement gradient tensor at a point. Accordingly, any displacement and corresponding gradient have to be defined as independent components on three perpendicular coordinate axes.

Fig. 1 shows two sphere and rectangular elements and a typical deformed shape of them. Obviously, there is a certain history of displacement on any random orientation through the element. These are abbreviated in three

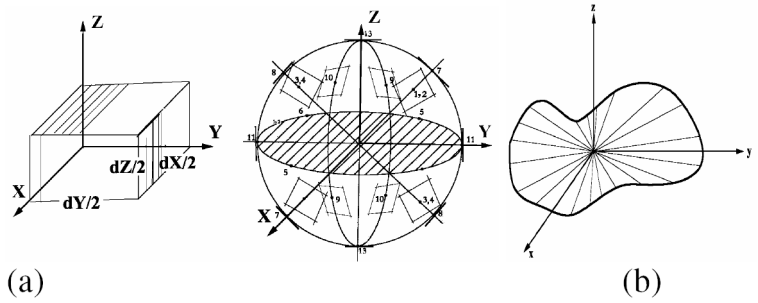

Fig. 1. a) Rectengular and sphere elements; b) Typical deformed elementnt [from sadrnejad 2005, 25]

directions when a rectangular-shape element is employed, and so, some directional information may be lost. To avoid missing any directional information of strain, one can employ a spherical element which carrying strain components over its surface seem more appropriate. This kind of strain approach will certainly represent a better distribution and includes all directional information. Certainly, to obtain the strain components as presented on planes of cubic element, strain variation is integrated over the sphere surface. However, a predefined numerical integration may be employed to reach the solution. Generally, numerical integration simulates the smooth curved sphere surface with a composition of flat tangential planes to make an approximated polygon to the sphere surface. Certainly the number of the sampling planes characterized the accuracy of the sphere surface approximation. Clearly, if the number of sampling planes is taken six, the approximated surface is the same as normal *dx, dy, dz* cubic element.

3. Multilaminate Frame Work

The concept of multilaminate models for granular materials is based on so-called integration or contact planes which have been introduced as sampling planes in last section. It has been assumed that the overall deformation behavior of granular materials could be achieved from an evaluation of deformations on these contact planes.

The multilaminate framework by defining small continuum structural units for assembling of grains and voids that fill infinite spaces between the contact planes, has appropriately justified the contribution of interconnection forces in overall macro-mechanics. Upon these suppositions, plastic deformations occur due to sliding, separation/closing of the boundaries and elastic deformations are the overall responses of these structural unit bodies. Therefore, Plastic equations are formulated on the contact planes and elastic equations on the whole volume as the common formulation of continuum mechanics. But in the present multilaminate model because of using unconventional plasticity assumption, there isn't any pure elastic domain for soil deformation in loading process, so deformation of soil is assumed elastoplastic from the first step of loading. Thus in the formulation presented here, elastic and plastic behavior are considered on the contact planes unlike the other usual multilaminate models. Therefore, the overall deformation of any small part of the medium is derived from an appropriate summation of elastoplastic sliding, separation/closing phenomenon of the sampling planes (contact planes). These assumptions simply imply that it is possible to have information about yielding/failure condition or even ill-conditioning and bifurcation response over any of the randomly oriented sampling planes for a point. Consequently, the granular material mass has an infinite number of yield functions for each orientation in the physical space.

Fig. 2 shows the real structural units of the soil body which will be replaced by the artificial polyhedrons. The created polyhedrons are roughly by 13 contact planes, passing through each point in the medium. The location of tip heads of normal directions of the planes,

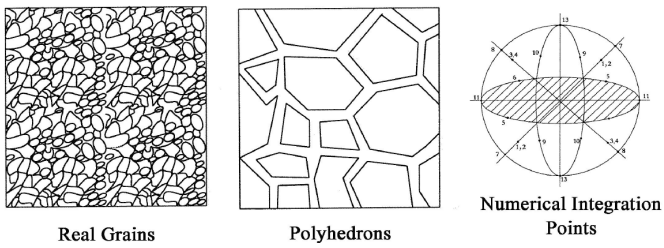

Fig. 2. Soil grains, artificial polyhydrones and sampling planes [from sadrnejad 2005, 25]

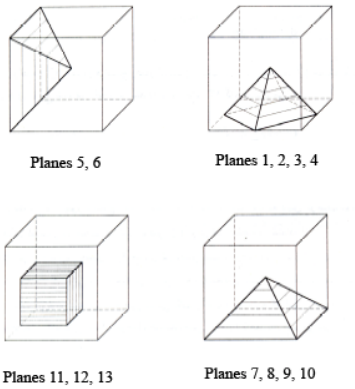

plane number	direction cosines of plane			weight coefficient
	L(i)	m(i)	n(i)	
1	0.577	0.577	0.577	0.0321
2	0.577	-0.577	0.577	0.0321
3	-0.577	0.577	0.577	0.0321
4	-0.577	-0.577	0.577	0.0321
5	0.707	0.707	0	0.0381
6	-0.707	0.707	0	0.0381
7	0.707	0	0.707	0.0381
8	-0.707	0	0.707	0.0381
9	0	-0.707	0.707	0.0381
10	0	0.707	0.707	0.0381
11	1	0	0	0.0476
12	0	1	0	0.0476
13	0	0	1	0.0476

Fig. 3. Demonstration, direction cosines and weighted coefficient of the 13 planes [from sadrnejad 2005, 25]

defining corresponding direction cosines of them, are shown on the surface of unit radius sphere.

In an ideal case, the overall behavior of the media will be achieved by normal integration for summing up the individual micro effects correspond to infinite number of micro sampling planes. But it is not possible to employ infinite number of planes, so the required integrals will be calculated with numerical methods by employing 13 sampling planes. The choice of 13 planes is a fair number for the solution of any three dimensional problem [6, 5]. The orientation of the sampling planes on the cubic element and direction cosines of normal directions on planes and weighted coefficients of them [26] for calculating the numerical integration rule and stress or strain tensors of each plane are shown in Fig. 3.

When implementing a multilaminate based model into a finite element code, the contact planes are located at each Gaussian point of the finite element mesh. In other word, there are 13 contact planes in each of the Gaussian point of the elements and the overall behavior of the points are achieved by valuation of the behavior of these planes. The constitutive equations for describing material behavior are formulated on the planes in local coordinates. Therefore, the stress state $\{\sigma\}$ at a Gaussian point must be transformed into normal and shear stresses (σ_n, τ *in Fig.* 4) on each plane utilizing a transformation matrix $[T_\sigma]$[*Eq.* (1)].

$$\begin{Bmatrix} \tau \\ \sigma_n \end{Bmatrix} = [T_\sigma] \{ \sigma \} \tag{1}$$

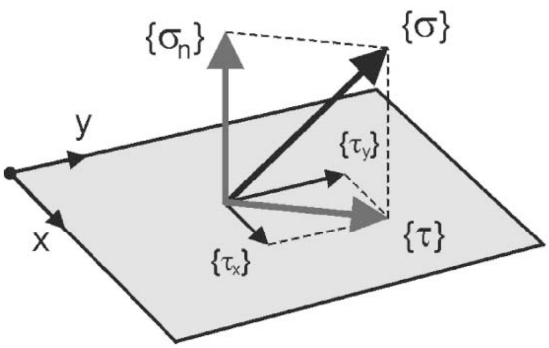

Fig. 4. Transformation of global stress {s} in integration point into local stresses {sn} and {t} on a contact plane.
[from Schuller & Schweiger 2002, 27]

Applying an elastoplastic formulation for contact planes, plastic volumetric and deviatoric strain rates $(\dot{\gamma}^p, \dot{\varepsilon}^p)$ could be calculated on each of the planes. Since the constitutive equations are defined on the level of the integration planes and formulated in two dimensional matter by terms of σ_n and τ, relatively simple mathematical expression can be used even to describe complex material behavior such as strain hardening and softening.

4. Constitutive Model for Sampling Planes

Deriving the constitutive equations of the subloading surface model, we should consider two surfaces; normal yield surface and subloading surface. The normal yield surface is the renamed form of the conventional yield surface, while its interior is not regarded as a purely elastic domain. In other word, in the subloading surface model there is no purely elastic deformation in the loading process. The subloading surface is introduced as a surface which always passes through the current stress point, while keeping a similar shape to the normal yield surface with respect to the origin of stress space, i.e. $\boldsymbol{\sigma} = 0$. The subloading surface is always within or on the normal yield surface. The following geometrical properties are the results of these features:

a. Each line connecting an arbitrary point on or within the subloading surface and its conjugate point on or within the normal yield surface joins at the similarity center which is the origin of the stress space in the present case.

b. Each ratio of the length of an arbitrary line, connecting two points on or inside the subloading surface to the length of another line which connects their conjugate points on or inside the normal yield surface is identical. This ratio is called similarity ratio, and it is equal with the ratio of the sizes of these surfaces.

The similarity ratio of the subloading surface to the normal yield surface might be named as normal yield ratio, R. Where R = 0, corresponds to the null stress state, 0 < R < 1, to the sub-yield state, and R = 1, to the normal yield state. In other word, where R = 0, size of the subloading surface is equal to zero, 0 < R < 1, it exists inside the normal yield surface and if R = 1, it will lie on the normal yield surface.

Before explanation of the equations for the multilaminate subloading surface model, it is worth noting that constitutive equations for the models which are described in the multilaminate framework, is worked in each of the planes separately. So as mentioned former the stress and strain vector have to be transported on these planes, $(\sigma^T = \{\tau \quad \sigma_n\} \& \varepsilon^T = \{\gamma \quad \varepsilon_n\})$. In addition, the strain rate of each plane, $\dot{\varepsilon}$, is decomposed into the elastic strain rate of the plane, $\dot{\varepsilon}^e$, and plastic strain rate of the plane, $\dot{\varepsilon}^p$:

$$\dot{\varepsilon} = \dot{\varepsilon}^e + \dot{\varepsilon}^p \tag{2}$$

Where the elastic strain rate is given by:

$$\dot{\varepsilon}_i^e = C^e \dot{\sigma} \tag{3}$$
$$C^e = \begin{bmatrix} 1/3G & 0 \\ 0 & 1/K \end{bmatrix}$$

Where K and G are the bulk and shear modulus of the planes respectively, which are functions of stress and internal state variables in general.

Assume the isotropic hardening/softening yield condition:

$$f(\sigma_y) = F(H) \tag{4}$$

Where the scalar H is the isotropic hardening/softening variable and σ_y is the stress state point on the normal yield surface. Assuming the function f is homogeneous of degree 1 in the stress field, the yield surface will be maintained a similar shape through the process.

The subloading surface can then be described as:

$$f(\sigma) = R\, F(H) \tag{5}$$

Where σ is the current stress state. In the formulation above we have $\sigma_y (= \sigma / R)$ and it is the conjugate stress point for σ on the normal yield surface, at which the outward normal is identical to outward normal of the current stress state on the

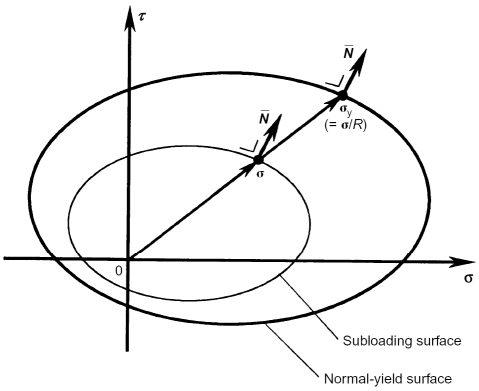

Fig. 5. Normal yield and subloading surfaces for each of the planes [from Hashiguchi et al. 2002,28]]

subloading surface. The normal yield and the subloading surface are illustrated in Fig. 5.

The time differentiation of equation 5 for the subloading surface is derived as:

$$\left(\frac{\partial f(\sigma)}{\partial \sigma}\right)^T \dot{\sigma} = \dot{R}\,F + R\,F'\dot{H} \tag{6}$$

Taking account of the fact that the current stress state approaches the normal yield surface during the loading process and the subloading surface have to carry this point to the normal yield surface, we need a rule to guarantee this evolution during loading process. let the evolution rule of the normal yield ratio, R, be given by

$$\dot{R} = U \left\|\dot{\varepsilon}^p\right\| \quad for\ \dot{\varepsilon}^p \neq 0 \tag{7}$$

Where U is a monotonically decreasing function of R (Fig. 6), satisfying the condition

$$\begin{cases} U = \infty & for\ R = 0 \\ U = 0 & for\ R = 1 \\ U < 0 & for\ R > 1 \end{cases} \tag{8}$$

These conditions are required to guarantee that the subloading surface approaches the normal yield surface during the loading process. Let the function U satisfying equation (8) be given by[17]

$$U = -u \ln R \tag{9}$$

Where u is a material parameter.

Substituting equation (7) into equation (6), *extended consistency* condition for the

$$\left(\frac{\partial f(\sigma)}{\partial \sigma}\right)^T \dot{\sigma} = U \left\|\dot{\varepsilon}^p\right\| F + R\,F\dot{H} \tag{10}$$

Assume the associated flow rule

$$\dot{\varepsilon}^p = \lambda\, \overline{N} \tag{11}$$

Where λ is the positive proportionality factor, and the vector $\overline{N}$ is the normalized outward normal of the subloading surface at the current stress state:

$$\overline{N} \equiv \frac{\partial f(\sigma)}{\partial \sigma} \Bigg/ \left\|\frac{\partial f(\sigma)}{\partial \sigma}\right\| \tag{12}$$

Substitution of equation (11) into equation (10) leads to

$$\lambda = \frac{(\overline{N})^T \dot{\sigma}}{M^p} \tag{13}$$

Where

$$M^p = \left(\frac{F'}{F}\overline{h} + \frac{U}{R}\right)\left[(\overline{N})^T \sigma\right] \tag{14}$$

$$\overline{h} \equiv \frac{\dot{H}}{\lambda}$$

Using the following relation based on the Euler's theorem for a homogeneous function:

$$\frac{\partial f(\sigma)}{\partial \sigma} = \left\|\frac{\partial f(\sigma)}{\partial \sigma}\right\| \overline{N} = \frac{\left(\frac{\partial f(\sigma)}{\partial \sigma}\right)^T \sigma}{(\overline{N})^T \sigma} \overline{N} = \frac{RF}{(\overline{N})^T \sigma} \overline{N} \tag{15}$$

plastic internal variables and $\overline{N}$ will keep in degree 1 since $\dot{H}$ is homogeneous of degree 1 of $\dot{\varepsilon}^p (= \lambda \overline{N})$. Notwithstanding adding the term U/R, the plastic modulus (Eq. (14)) in the present model remained simple.

The plastic strain rate is given from equations (11) and (13) as

$$\dot{\varepsilon}^p = \frac{\overline{N}^T \dot{\sigma}}{\overline{M}^p} \overline{N} \tag{16}$$

Substituting of equations (3) and (15) into equation (2) gives the strain rate:

$$\dot{\varepsilon} = C^e \dot{\sigma} + \frac{\overline{N}^T \dot{\sigma}}{\overline{M}^p} \overline{N} \tag{17}$$

The loading criterion is given as follows [23]:

$$\begin{cases} \overline{N}^T D^e \dot{\varepsilon} > 0 \rightarrow \dot{\varepsilon}^p \neq 0 \\ \overline{N}^T D^e \dot{\varepsilon} \leq 0 \rightarrow \dot{\varepsilon}^p = 0 \end{cases} \tag{18}$$

The modulus matrix of each plane could be calculated as:

$$C^p = \frac{1}{\overline{M}^p} \overline{N}\ \overline{N}^T \tag{19}$$

$$C^{ep} = C^e + C^p$$

The matrix obtained from equation (19) is but common modulus matrix which is used in finite element method should be . Following equation facilitates the transformation:

$$\left[C^{ep}\right]_{6\times6} = \left[T\right]_{6\times2} \left[C^{ep}\right]_{2\times2} \left[T\right]^T_{2\times6} \tag{20}$$

$$\mathbf{T}^T = \begin{bmatrix} \frac{\partial \tau}{\partial \sigma_x} & \frac{\partial \tau}{\partial \sigma_y} & \frac{\partial \tau}{\partial \sigma_z} & \frac{\partial \tau}{\partial \sigma_{yz}} & \frac{\partial \tau}{\partial \sigma_{zx}} & \frac{\partial \tau}{\partial \sigma_{xy}} \\ \frac{\partial \sigma_n}{\partial \sigma_x} & \frac{\partial \sigma_n}{\partial \sigma_y} & \frac{\partial \sigma_n}{\partial \sigma_z} & \frac{\partial \sigma_n}{\partial \sigma_{yz}} & \frac{\partial \sigma_n}{\partial \sigma_{zx}} & \frac{\partial \sigma_n}{\partial \sigma_{xy}} \end{bmatrix}$$

A general modulus matrix of a point is then calculated as:

$$\left[C^{ep}\right]_{6\times6} = 8\pi \sum_{i=1}^{13} w_i \left[C_i^{ep}\right]_{6\times6} \tag{21}$$

i = plane number

Mechanism of dilation behavior controls in this model with critical state line. Critical state line identifies the pick of subloading surface (and so normal yield surface because of similarity). The normal of the subloading surface don't have any component in the volumetric strain direction on the its pick, so there is no change in the volume of the sample. The volumetric component of the normal of subloading surface at the left-hand side of the pick point is negative and it is positive at the write-hand side of the pick point (Fig. 7).

The size of subloading and normal yield surface decrease in the softening process but the normal yield ratio increases, so the plastic strain develops while the stress state decreased . In the hardening behavior, the size of these surfaces and the normal yield ratio increase and the hardening behavior is modeled simply. So the model can simulate hardening and softening behavior without any additional hypothesis.

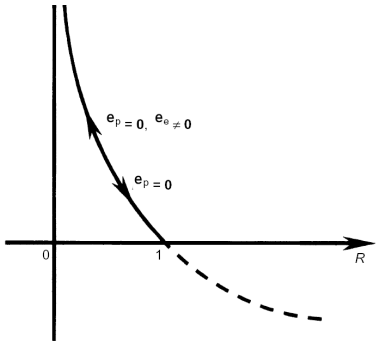

Fig. 6. The function U in the evolution rule of the normal yield ratio, R [from Hashiguchi et al. 2002, 25]

The plastic strain rate (equation (16)) is obtained by substituting the associated flow rule (equation (11)) into the extended consistency condition (equation (10)), which is obtained by incorporating the evolution rule of the normal yield ratio, R, (equation (7)), into time differentiation (equation (6)) of equation (5) for the subloading surface. The plastic deformation then develops gradually as the stress approaches the normal yield surface and exhibits a smooth elastic-plastic transition. Thus the subloading surface model fulfills the *smoothness condition [21,22,23]*, which defines the stress rate/strain rate relation changing continuously for a continuous change of stress state. This can be expressed mathematically as:

$$\lim_{\partial\sigma_i \to 0} \frac{\partial \dot{\sigma}\ (\sigma + \delta\sigma, S_j, \dot{\varepsilon})}{\partial \dot{\varepsilon}_i} = \frac{\partial \dot{\sigma}\ (\sigma, S_j, \dot{\varepsilon})}{\partial \dot{\varepsilon}} \tag{22}$$

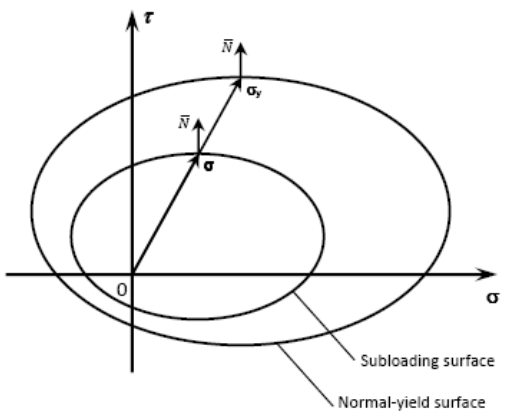

Fig 7. Subloading surface, and normal-yield surface and the pic point for dilation control

Where $S_j (j = 1,2,3,...,m)$ denotes collectively scalar or tensor-valued for internal state variables describing the alteration of mechanical response property due to the irreversible deformation, $\delta()$ stands for an infinitesimal variation, and the response of the stress rate to the strain rate in the current state of stress and internal variables is designated by $\dot{\sigma}\ (\sigma, S_j, \dot{\varepsilon})$. This is a feature of subloading surface model which has been mentioned by Hashiguchi and Chen [24].

The subloading surface constitutive equations within the multilaminate framework have the following notable advantages:

a. It predicts a smooth response (for example a smooth relation between deviatoric stress and axial strain under uniaxial loading) for smooth monotonic loading. By contrast, a non-smooth response is predicted by constitutive models violating the smoothness condition, for example one can see a none smooth curve at the yield point of the conventional elastic-plastic constitutive model.
b. The only judgment required in the loading criterion of the constitutive equation in each plane is the sign of equation (18), since the stress always lies on the subloading surface, which just plays the role of the loading surface.
c. In this model a stress state will be automatically drawn back to the normal yield surface even if goes out from it, since it is formulated that $\dot{R} > 0$ for $R < 1$ (subyield state) and $\dot{R} < 0$ for $R > 1$ (over the normal yield state). Thus a rough numerical calculation with a large loading step is allowed in the subloading surface constitutive equation.
d. This model can easily simulate induced anisotropic behavior of the material without any additional hypothesis. Since the formulation in each of the planes works separately and stress/strain path can be different in each of the planes.
e. By defining different material parameters in each plane, this model can simulate inherent anisotropy too. But it is a potential feature of this model and need some consideration for calculating the initial value of parameters on each of the planes.
f. By controlling the amount of stress and strain in each plane, one can identify the direction of probable cracks and slides in a material body.

4. 1. Application to Soils

The particular forms of the material functions for soils are given in this section. The isotropic hardening/softening function, F, is given by[28]

$$F = F_0 \exp(\frac{H}{\rho - \gamma}) \tag{23}$$

Where F_0 is the initial value for F, ρ and γ are the slopes of the normal consolidation and the swelling curves respectively in $\ln \nu - \ln p$ space (where in ν is the volume and $p \equiv tr(\sigma)/3$ is pressure) [25,7].

In the classical continuum mechanics it is common to describe the evolution of the isotropic hardening/softening variable with volumetric plastic strain. So the isotropic hardening/softening variable in this model is connected with normal plastic strain which plays the role of volumetric plastic strain in the multilaminate based model, in its simplest form. Therefore, the evolution rule of the isotropic hardening/softening variable H is given as

$$\dot{H} = \dot{\varepsilon}_n^p \tag{24}$$

The elastic shear modulus, G, is given from the elastic bulk modulus, K, and Poisson's ratio, ν, as

$$G = \frac{3K(1-2\upsilon)}{2(1+\upsilon)} \tag{25}$$

and the relevant elastic constitutive equation of soils has been proposed recently by Hashiguchi & Collins [29].

The subloading surface equation is given as

$$f(\sigma) = (\sigma_n) + \frac{2}{3} \times \frac{\tau}{m\ (\sigma_n)} = R\ F(H) \tag{26}$$

Where m is a material parameter which is describing the stress ratio in the critical state line.

5. Determination of Material Parameters

As seen before, the proposed model has six material parameters (five material parameters and one initial value: F_0) which have to be calibrated through experiments. The determination of six material parameters $\rho,\ \gamma,\ F_0,\ \upsilon,\ u$ and m is calculated the same as the subloading surface model which has been introduced by Hashiguchi et al. [28] and would be explained briefly here.

The material constants ρ, γ, and F_0 are evaluated from the results of isotropic consolidation test data which have been depicted in the logarithmic diagram of both pressure and volume. In this diagram, ρ can be determined with the slopes of normal consolidation line, γ with the slopes of swelling line and F_0 with the pressure at the transitional point of the swelling line and normal consolidation line. If the consolidation test data are not available, Odeometric test data can be used for determination of these parameters.

Poisson's ratio, ν, is evaluated from triaxial compression test with constant lateral stress, by fitting the axial stress-strain curve with the inclination of the initial rising part of the test data.

The material constant, *u*, in the evolution rule of the normal yield ratio *R* can be calculated with fitting the curvature of the stress-strain curve in transitional state.

The material constant, *m*, describes the stress ratio in the critical state line. It can be evaluated from the stress ratio in the residual state of the triaxial compression test data.

6. Comparison with Test Data

In order to scan the ability of the present model in prediction of the real soil behavior in an acceptable way, the simulation results in several series of test data for sands and clays under the drained and undrained conditions are shown in this section. The drained results are compared with three sets on test data and undrained behavior is compared with two sets of test data.

A single test data for presenting the power of the model in prediction of softening behavior of soils is compared separately.

6. 1. Drained Test

The test results of Hostun sand are selected at first [30]. These tests were conducted with true triaxial apparatus under isotropic loading, axisymmetric compression with a constant lateral stress ($\sigma_x = \sigma_y = 200\ kPa \le \sigma_z$) , axisymmetric extension with a constant lateral stress ($\sigma_x = \sigma_y = 200\ kPa \le \sigma_z$) and circular stress path in the deviatoric stress plane. The last test split into two stages:

a) The axial stress σ_z was increased to 842 kPa from the isotropic stress state of 500 kPa, while σ_x and σ_y were both decreased proportionately to 329 kPa. This procedure kept the mean stress σ_m in 500 kPa. The magnitude of deviatoric stress $\|\sigma^*\|$ at the end of this stage became 420 kPa.

b) A circular stress path(lode's angle was varied from 60° to 180°) was exerted in the deviatoric stress plane by varying three principal stresses $\sigma_x,\ \sigma_y,\ \sigma_z$, while σ_m and $\|\sigma^*\|$ was kept constant.

The Hostun sand used for the tests is a poorly graded material with similar grain size distribution. Tests were done in the dense state with the initial void ratio $e_0 = 0.616$.

The following material parameters and initial values are used for modeling the behavior of Hostun sand:

$$\rho = 0.5,\ \gamma = 0.0003,\ \upsilon = 0.4,\ m = 0.06$$

$$u = 105,\ ,F_0 = 6000\ kPa$$

Figs. 8, 9 and 10 are shown the comparison of the tests data and calculated results. It is common in modeling of the soil behavior to use of non associated flow rule because of specific behavior of the soil in volumetric deformation. Whereas adoption of associated flow rule in this model has predicted realistic behavior even for volumetric deformation of the soils.

Fig. 11 shows the variations of the principal strains $\varepsilon_x,\ \varepsilon_y,\ \varepsilon_z$ and the volumetric strain ε_v vs. lode's angle θ_σ for the circular stress path. The totality of the shapes of the predicted curves and experimental curves are almost identical, but there are differs in their values and inclinations

which might be better if more sampling planes is employed [27].

The subloading surface model cannot simulate the circular stress path. This is one of the benefits of implementation in the multilaminate framework. Because the model which proposed by Hashiguchi et al. [28] works with $\|\sigma^*\|$ and σ_m (as the stress invariants) and there is no change in these invariants in the mentioned circular stress path. But in the present model any variation of the stress tensor components will change the normal or shear stress on some of the planes, so it can simulate this circular stress path easily.

The second and third sets are the results of Nevada sand [31]. These tests are conducted with true triaxial apparatus too, but under different constant confining pressures of 40, 80 and 160 kPa. The sand samples were prepared in two different initial void ratios: 0.65 and 0.72.

The following material parameters and initial values are used in the calculations:

$\rho = 0.7$, $\gamma = 0.0001$, $\upsilon = 0.4$, $m = 0.055$,

$u = 125$, $F_0 = 3.5 \times P_0$ $KPa \rightarrow for$ $e_0 = 0.72$

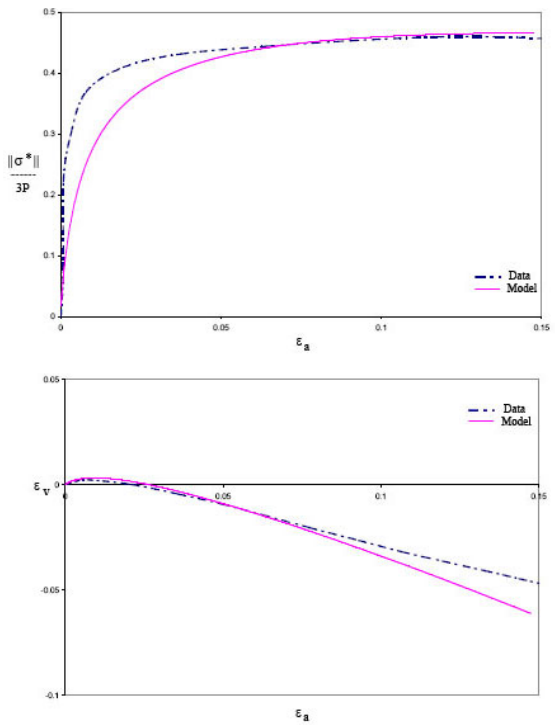

Fig 9. Comparison result for Hostun sand under axsysimetric compression loading

$\|\sigma^*\|$: magnitude of deviatoric stress tensor

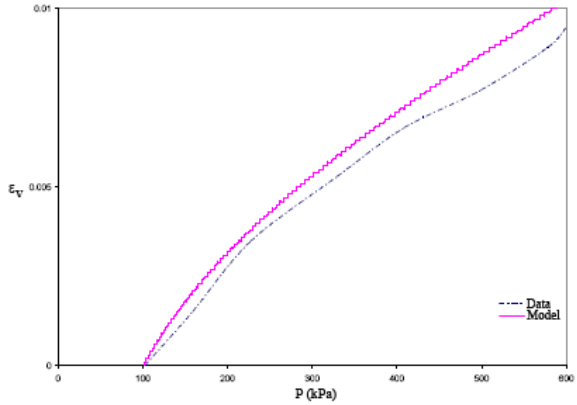

Fig. 8. Comparison result for Hostun sand under isotropic loading

$\rho = 0.9$, $\gamma = 0.0001$, $\upsilon = 0.4$, $m = 0.058$,

$u = 145$, $F_0 = 4.0 \times P_0$ $KPa \rightarrow for$ $e_0 = 0.65$

Figs. 12 and 13 are shown the comparison results of the tests data and calculated curves. Good agreements with the experimental results are achieved at all samples and with different confining pressures under the drained condition.

The stress-strain and volumetric strain vs. axial strain curves predicted by purposed model are compared with the test data for kaolinite-silt

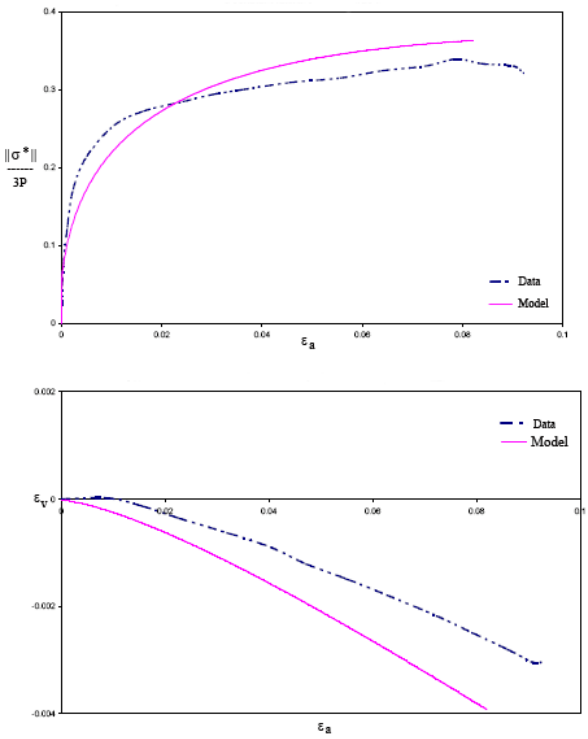

Fig. 10. Comparison result for Hostun sand under axisymetric extension loading

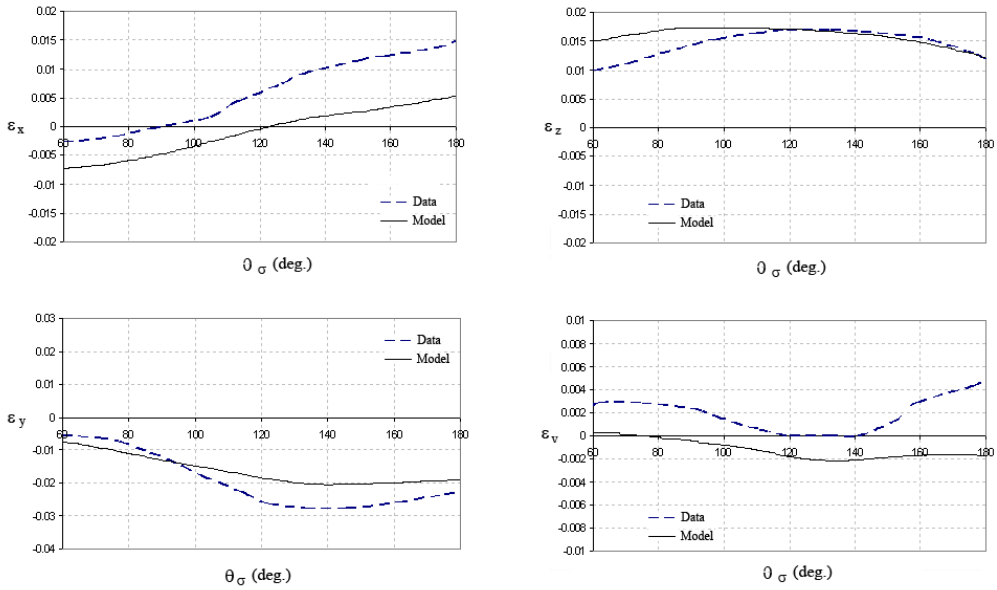

Fig. 11. Comparison results for Houston Sand under the loading of circular stress path in the deviatoric stress plane

mixture [32]. This is shown in Fig. 14 for presenting the power of the model in prediction the softening behavior of soils. The following material constants and initial values are used in the calculations:

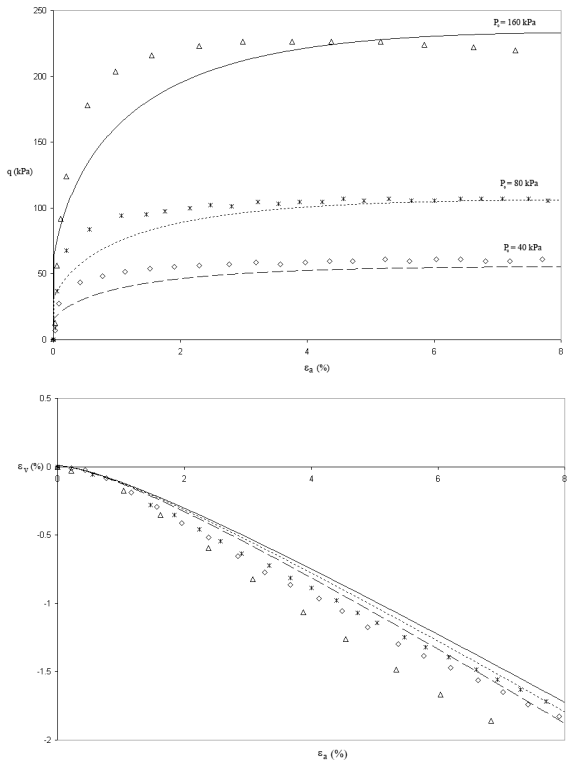

Fig. 12. Comparison result for nevada sand by e = 0.72 under three diffrent constant-p test

$$\rho = 0.052,\ \gamma = 0.0005,\ \upsilon = 0.3,\ m = 0.145$$

$$,\ u = 170,\ ,F_0 = 6300\ kPa$$

As noted earlier, in the softening behavior the size of the normal yield and subloading surfaces are decrease while the normal yield ratio is increase. Reduction of the size of these surfaces cause the stress state to decrease while increase of normal yield ratio develops the plastic strain.

Fig. 15 shows the power of the model in simulation of anisotropic behavior. Shear stress vs. shear strain curve in plane 1 and 10 for Kaolinite-silt mixture is presented in this figure. As shown in these curves, soil behavior in plane 1 is not the same as in plane 10. So we can say that depend on the applied stress-path, this model can consider different plastic deformations in 13 directions. Consequently influence of induced anisotropy can be simulated very simply and without any additional hypotheses.

The feature of this model which cannot find in Hashiguchi et al. [28] is the power of the model in simulation of anisotropy. However Hashiguchi and Chen [24] proposed a subloading surface model with rotational hardening for describing anisotropic behavior, their model is so complicated to use, but this model is very simple.

Soil behavior is change due to plastic deformation, and it's the key point in the induced anisotropic behavior. In the loading process the

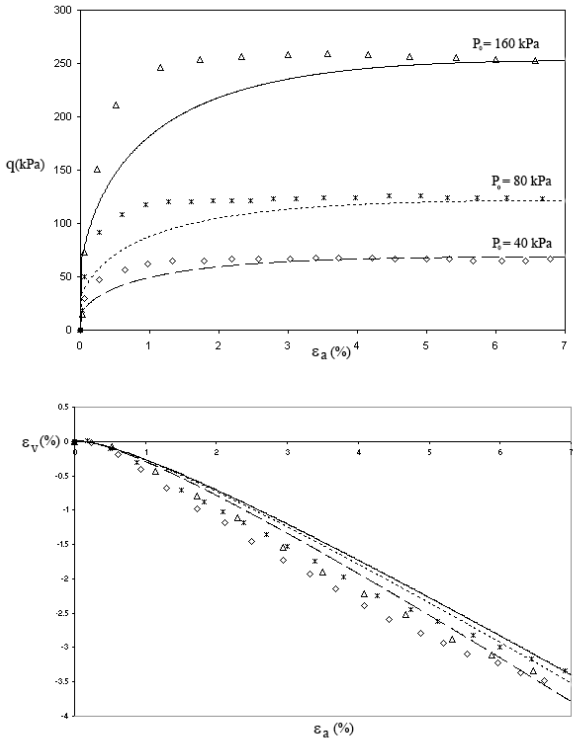

Fig. 13. Comparison result for nevada sand by e_c= 0.65 under three diffrent constant-p test

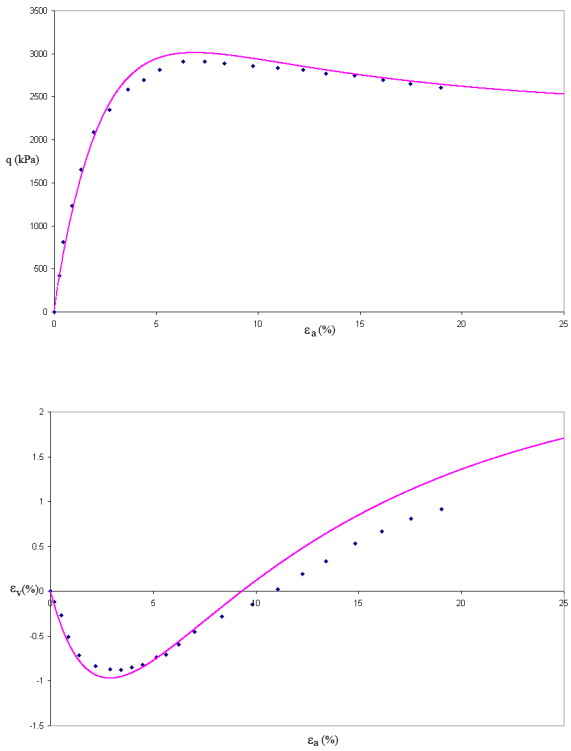

Fig. 14. Comparison result for kaolinite-silt mixture under darined triaxial compression test with constant lateral pressure

soil medium will experience different plastic deformation in different directions and so it behaves differently in special directions. In common continuum mechanics, there is one yield and potential surface for describing the behavior, and so plastic variables will be unique for the whole volume in each step of loading. But in the multilaminate frame work, we have 13 (or more) planes with 13 individual yield and potential surface and plastic variables on these planes will change individually due to the plastic strain of these planes. Consequently the media behaves differently in different directions and induced anisotropy can be accounted automatically.

In addition, common models employ some invariants of the stress or strain instead of stress/strain tensors for describing the behavior, and we know using these variables will lose some information of the tensors. Because there are various stress paths which don't change the invariant while the stress tensor has changed.

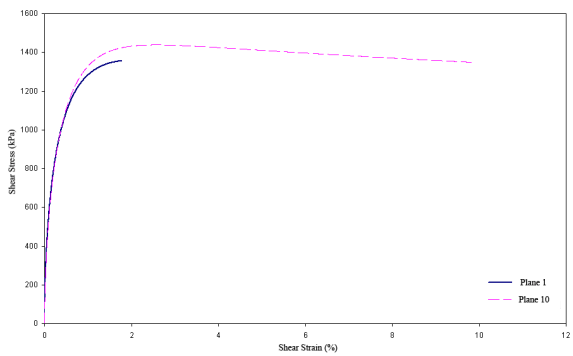

Fig. 15. Stress - strain curves for Koalinite-silt mixture in planes 1 & 10

6. 2. Undrained Tests

The results of the proposed model under undrained condition are examined in this section. The stress paths and stress-strain curves are compared with the test data for Red Clay [33] subjected to the undrained triaxial compression test. These tests were conducted with different confining pressures. Fig. 16, shows the comparison results. The material parameters and the initial value are selected as follows:

$$\rho = 0.04,\ \gamma = 1.2E-4,\ \upsilon = 0.2\ ,m = 1.015\ ,$$

$$,\ u = 110,\ ,F_0 = 300\ \ kPa$$

A similar comparison for test data of London clay [34] is shown in Fig. 17. The material

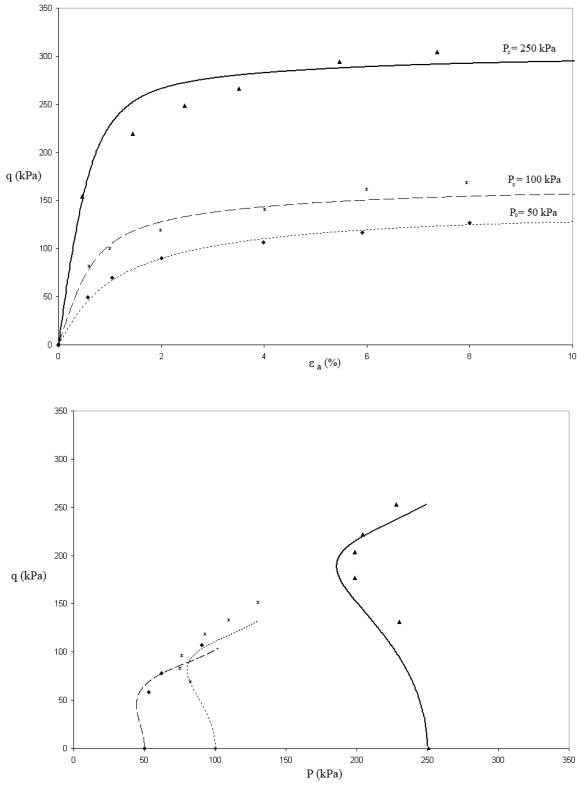

Fig. 16. Comparison result for Red Clay under undarined triaxial compression test with constant lateral pressure

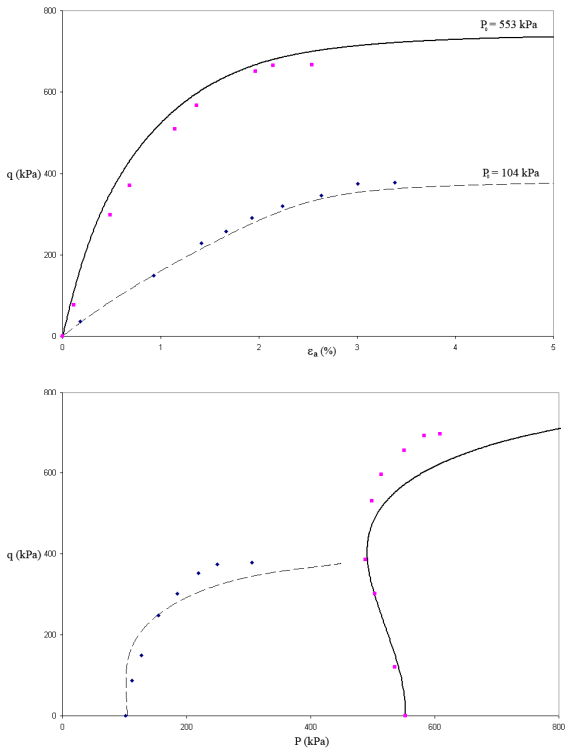

Fig. 17. Comparison result for London Clay under undarined triaxial compression test with constant lateral pressure

parameters and the initial value are for these cases are selected as follows:

$$\rho = 0.025,\ \ \gamma = 6.5e-5,\ \ \upsilon = 0.1\ \ , m = 0.72$$

$$,\ \ u = 215,\ \ , F_0 = 2500\ \ kPa$$

Reasonable agreement for undrained tests with different confining pressures is achieved too.

7. Conclusion

A simple unconventional elastoplastic constitutive model was developed within the multilaminate framework in this study. This model can consider the influence of anisotropy in a rational way and without any additional hypotheses. The multilaminate based models can also consider the effect of rotation of principle stress axis in the elastic-plastic deformation of materials.

This model is able to solve a three dimensions plasticity problems by a rather simple theory based on the phenomenological description of two dimensions plastic deformation and isotropic hardening/softening of materials. This is actually achieved in such a way that the application of some difficult tasks such as anisotropy and rotation of principal stress and strain axes (where there may be not co-axiality of them), to be predictable. Accordingly, constitutive formulations on the sampling planes provide convenient means to classify loading events, generate history rules and independent evolution rules for local variables.

The purposed model was applied to predict the deformation behavior of sands and clays under drained and undrained conditions, and thus its applicability was verified.

References

[1] Christofferson, C., Mehrabadi, M.M., Nemat-Naser, S.A. (1981), "Micromechanical description of granular behavior", J. Appl. Mech., ASME, Vol. 48, 339-344.

[2] Nemat-Naser, S.A., Mehrabadi, M.M (1983), "Stress and fabric in granular masses", Mechanics of granular materials, New models and constitutive relations (Eds. J.T. Jenkins and M. Satake), Elsevier Sci. Pub., 1-8.

[3] Schwieger, H.F., Schuller, H., "New development and practical applications of the multilaminate model for soils", Smith & Carter (eds.) Proc. Developments in theoretical Geomechanincs. The John Booker Memorial Symposium Sydney: 329- 350. Rotterdam: Balkema.

[4] Zeinkiewicz, O.C., Pande, G.N. (1977), "Time dependent multilaminate model of rocks- a numerical study of deformation and failure of rock masses", Int. J. Numer. Anal. Methods Geomech., Vol. 1, 219- 247.

[5] Pande, G.N., Sharma, K.G. (1983), "Multilaminate of clays- a numerical evaluation of the influence rotation of principal stress axis", Int. J. Numer. Anal. Methods Geomech., Vol. 7, 397- 418.

[6] Krajewski, W. (1986), "Mathematisch-numerische und experimentelle Untersuchungen zur Bestimmung der Tragfahigkeit von in Sand gegrundeten, vertikal belasteten Pfahlen", Veroffentlichungen des Instituts fur Grundbau, Bodenmechanik, Felsmechanik, und Verkehrswasserbau der RWTH Aachen, Heft.

[7] Sadrnejad, S. A., Pande, G.N. (1989), "A multilaminate model for sands", Proceeding of 3rd International Symposium on Numerical Models in Geomechanics, NUMOG III, Niagara Falls, Canada.

[8] Pietruszczak, S., Pande, G.N. (1987), "Multilaminate framework of soils models-plasticity formulation", Int. J. Numer. Anal. Methods Geomech., Vol. 11, 651- 658.

[9] Karstunen, M. (1999), "Numerical modeling of strain localization in dense sands", Acta Polytechnica Scandinavica No. 113. Espoo. The Finnish Academy of Technology.

[10] Bazant, Z.P., Prat, P.C. (1988), "microplane model fro brittle-plastic material: I. theory", Journal of Eng. Mechanics, Vol. 114, 1672-1688.

[11] Iwan, W.D. (1967), "On a class of models for the yielding behavior of continues and composite systems", J. Appl. Mech., ASME, Vol. 34, 612-617.

[12] Mroz, Z. (1966), "On forms of constitutive laws for elastic-plastic solids", Archiwum Mechaniki Stosowanej, Vol. 18, 1- 34.

[13] Mroz, Z. (1967), "On the description of anisotropic work hardening", J. Mech. Phys. Solids, Vol. 15(2), 163- 175.

[14] Mroz, Z., Norris, V.A., Zeinkiewicz, O.C. (1981), "An anisotropic, critical state model for soils subjected to cyclic loading", Geotechnique, Vol. 31(4), 451- 469.

[15] Dafalias, Y.F., Popov, E.P. (1975), "A model of nonlinearly hardening materials for complex loading", Acta. Mech., Vol. 21, 173- 192.

[16] Krieg, R.D. (1975), "A practical two surface plasticity theory", J. Appl. Mech., ASME, Vol. 42(3), 641- 646.

[17] Hashiguchi, K. (1980), "Constitutive equations of elastoplastic materials with elastic-plastic transition", J. Appl. Mech., ASME, Vol. 47(2), 266- 272.

[18] Hashiguchi, K. (1989), "Subloading surface model in unconventional plasticity", Int. J. Solids Struct.", Vol. 25(8), 917- 945.

[19] Hashiguchi, K., Ueno, M. (1977), "elastoplastic constitutive laws of granular materials", Constitutive equation of soils Proc. 9th Int. Conf. Soil Mech. Found. Eng., Special session 9, Tokyo, 73- 82.

[20] Hashiguchi, K. (1993a), "Fundamental requirements and formulation of elastoplasic constitutive equations with tangential plasticity", Int. J. Plasticity, Vol. 9 (5), 525- 549.

[21] Hashiguchi, K. (1993b), "Mechanical requirements and structures of cyclic plasticity models", Int. J. Plasticity, Vol. 9 (6), 721- 748.

[22] Hashiguchi, K. (1997), "The extended flow rule in plasticity", Int. J. Plasticity, Vol. 13 (1), 37-58.

[23] Hashiguchi, K. (2000a), "Fundamentals in constitutive equation: continuity and smoothness conditions and loading criterion", Soils Found., Vol. 40 (3), 155- 161.

[24] Hashiguchi, K., Chen, Z.P. (1998), "Elastoplastic constitutive equations of soils with the subloading surface and the rotational hardening", Int. J. Numer. Anal. Methods Geomech., Vol. 22 (3), 197- 227.

[25] Sadrnejad, S. A. (2005), "Fabric behavior of sands in post-liquefaction", American Journal of Applied sciences, Vol. 2 (12), 1562- 1573.

[26] Abramowitz, M., Stegun, I.A. (1965), "Handbook of Mathematical Functions", Dover Publications, Inc., New York.

[27] Schuller, H., Schweiger, H. F. (2002), "Application of multilaminate Model to Simulation of Shear Band Formation in NATM-Tunneling", Computers and Geotechnics, Vol. 29(7), 501-524.

[28] Hashiguchi, K., Saitoh, K., Okayasu, T., Tsutsumi, S. (2002), "Evaluation of Typ-ical Conventional and Unconventional Plasticity Models for Prediction of Softening Behavior of Soils", Geotechnique, Elsevier, Vol. 52(8), 561-578.

[29] Hashiguchi, K., Collins, I.F. (2001), "Stress rate-elastic stretching relations in elastoplastic constitutive equations", Soils Found., Vol. 41 (2), 77- 87.

[30] Saada, A.S., Bianchini, G. (eds), Proc. Int. Workshop on Constitutive Equations for granular Non-cohesive soils, Cleveland, Balkema, Rotterdam, 1989.

[31] Arumoli, K., Muraleetharan, K.K., Hossein, M.M., Fruth, L.S. (1992). VELACS: verification of liquefaction analysis by centrifuge studies – laboratory testing program, soils data report. Earth Technology Corporation. Also available from university of Southern California web site, http:// rccgO1.usc.edu/eqdata/home.html.

[32] Stark, T.D., Ebeling, R.M., Vettel, J.J. (1994), "Hyperbolic stress-strain parameters for silts", J. Geotech. Eng., ASCE, Vol. 120(2), 420- 441.

[33] Wesley, L.D. (1990), "influence of structure and composition of residual soils", J. Geotech. Eng. ASCE, Vol. 116(4), 589- 603.[34] Bishpo, A.W., Webb, D.L., Lewin, P.I. (1965), "Undisturbed samples of London clay from the Ashford Common shaft: strenghth- effective stress relationship", Geotechnique, Vol. 15(1), 1- 31.

[34] Bishpo, A.W., Webb, D.L., Lewin, P.I. (1965), "Undisturbed samples of London clay from the Ashford Common shaft: strenghth- effective stress relationship", Geotechnique, Vol. 15(1), 1- 31.